NI

CR-166210

LIDAR MEASUREMENTS OF THE POST-FUEGO STRATOSPHERIC AEROSOL

Prepared by

PHILIP B. RUSSELL, RICHARD D. HAKE, JR., and WILLIAM VIEZEE
STANFORD RESEARCH INSTITUTE
MENLO PARK, CALIFORNIA 94025

April 1976

Supported by

CIAP OFFICE
U.S. DEPARTMENT OF TRANSPORTATION
WASHINGTON, D.C. 20590

Prepared under Contract NAS2-8674

for

AMES RESEARCH CENTER
NATIONAL AERONAUTICS AND SPACE ADMINISTRATION
MOFFETT FIELD, CALIFORNIA 94035

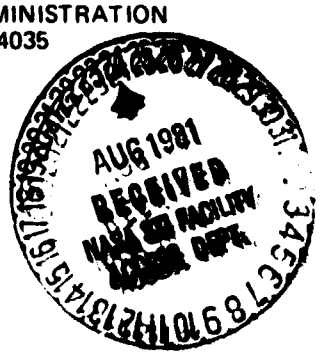

STANFORD RESEARCH INSTITUTE
Menlo Park, California 94025 · U.S.A.

STANFORD RESEARCH INSTITUTE
Menlo Park, California 94025 · U.S.A.

Final Report *April 1976*

LIDAR MEASUREMENTS OF THE POST-FUEGO STRATOSPHERIC AEROSOL

Prepared by

PHILIP B. RUSSELL, RICHARD D. HAKE, JR., and WILLIAM VIEZEE
STANFORD RESEARCH INSTITUTE
MENLO PARK, CALIFORNIA 94025

Supported by

CIAP OFFICE
U.S. DEPARTMENT OF TRANSPORTATION
WASHINGTON, D.C. 20590

Prepared under Contract NAS2-8674

SRI Project 4019

Approved by

R. T. H. COLLIS
RAY LEADABRAND

for

AMES RESEARCH CENTER
NATIONAL AERONAUTICS AND SPACE ADMINISTRATION
MOFFETT FIELD, CALIFORNIA 94035

ABSTRACT

Fifteen lidar observations of the stratospheric aerosol were made between February and November 1975. All observations revealed the greatly increased particulate backscattering that followed the eruption of the volcano Fuego in October 1974. Vertical structure consisted initially of multiple layers, which later merged to form a single, broader peak. Essentially all of the increased scattering was confined to altitudes below 20 km. Hence, aerosol layer centroids in 1975 were typically several km below their altitude prior to the eruption.

Our observations began in mid-February, at about the time of maximum northern midlatitude influence of the volcanic injection. From late February on, both vertically integrated particulate backscattering and the peak ratio of particulate to gaseous backscattering displayed approximately exponential declines, with mean lifetimes (1/e-lives) of eight and eleven months, respectively. These relatively short residence times are a combined consequence of the low altitude of the volcanic particles and their larger mean size as compared to the preinjection, or unperturbed, aerosol. The peak scattering ratio of our average 1975 profile was 1.7, and the vertically integrated particulate backscattering was 3.6×10^{-4} sr^{-1} (both at $\lambda = 694$ nm). The mean midvisible particulate optical thickness, derived from measured backscattering and realistic optical models,

was about 0.03, approximately six times the mean value in the year before the Fuego eruption, but not as large as values observed for some years after the 1963 Agung eruption.

Radiative and thermal consequences of the measured post-Fuego layer were computed using several recently published models. The models predict a temperature increase of several °K at the altitude of the layer, caused by the infrared absorption bands of the sulfuric acid particles. The surface temperature decrease predicted by the models is considerably smaller than 1°K, partly because of the small optical thickness of the volcanic layer, and partly because of its short residence time relative to the earth-ocean thermal response time.

CONTENTS

ABSTRACT ii

LIST OF ILLUSTRATIONS v

LIST OF TABLES vi

1. INTRODUCTION 1

2. INSTRUMENTATION AND DATA ANALYSIS 3

3. RESULTS 6

4. DISCUSSION 24

a. Temporal development of aerosol structure 24
b. Radiative and thermal effects 27
c. Accuracy of the lidar results 38

5. SUMMARY 41

ACKNOWLEDGMENTS 43

REFERENCES 44

ILLUSTRATIONS

1. Vertical Profiles of Scattering Ratio Measured by the Ruby Lidar in 15 Observations, February-November 1975 7

2. Vertical Profiles of Scattering Ratio Measured Between 11 and 13 November 1975 9

3. Time Variation of Altitude of Maximum Scattering Ratio, Centroid of (R-1) and Centroid of Particulate Backscattering, February-November 1975 11

4. Time Variation of Vertically Integrated Particulate Backscattering and Maximum Scattering Ratio, February-November 1975 13

5. Comparison of Lidar and Balloon-Borne Particle Counter Measurements of the Stratospheric Aerosol, 1963-1975 15

6. Average Vertical Profile of Scattering Ratio Measured over Central California Coast, February-November 1975 18

7. Average Vertical Profiles of Scattering Ratio Observed in Three Ruby Lidar Studies of the Stratospheric Aerosol Between 1964 and 1975 19

8. Profiles of Stratospheric Turbidity (Ratio of Particulate to Gaseous Extinction) Derived from the Present Series of Lidar Observations and from a Searchlight Measurement in Late 1974 (Elterman, 1975) 22

TABLES

1. Particulate Optical Thickness, τ, Between 10 km and Listed Altitude, for a Wavelength $\lambda \approx 550$ nm 23

2. Radiative and Thermal Effects of Stratospheric Aerosol Layers, as Predicted by Several Recent Models 29

3. Particle Characteristics and Modeling Methods Used in the Models Cited in Table 2 30

4. Radiative and Thermal Effects of a Stratospheric Aerosol Layer with Mid-Visible Optical Thickness $\tau = 0.030$ as Predicted by the Models in Tables 2 and 3 34

1. Introduction

In October 1974 the volcano Fuego in Guatemala (14.5°N, 91°W) erupted violently over a period of several days (Smithsonian, 1974). The eruption plume penetrated into the stratosphere, and very shortly thereafter dramatic twilight effects were observed at many northern hemisphere locations as the cloud was transported by the stratospheric circulation (e.g., Meinel and Meinel, 1974; Fegley and Ellis, 1975; Volz, 1975). Sudden increases in the numbers, mass, and optical backscattering and extinction of stratospheric particles were measured by balloon-borne counters, aircraft-borne samplers, ground-based lidars, and a spacecraft-borne radiometer at a variety of locations (e.g., Hofmann and Rosen, 1976; Ferry and Lem, 1975; Lazrus et al., 1975; Remsberg and Northam, 1975; McCormick and Fuller, 1975; Fegley and Ellis, 1975; Fernald and Frush, 1975a,b; Hirono et al., 1975; Pepin, 1975). At northern midlatitudes, both the numbers of particles and their optical backscattering were observed to increase very irregularly until about February 1975, after which a more regular decline began.

This paper describes stratospheric lidar measurements made at Menlo Park, California (37°N, 122°W) between mid-February and mid-November 1975. The measurements thus began when the influence of the Fuego injection was near its peak in northern midlatitudes, and they trace the subsequent decline and tendency toward pre-Fuego conditions. The measurements were an extension of a pre-Fuego observation series

that has been described elsewhere (Russell et al., 1974, 1976a,b). The purpose of this paper is to document the 1975 decline in stratospheric aerosol content, to compare our post-Fuego lidar measurements to pre- and post-Fuego measurements made by a variety of methods, and to derive some conclusions about the radiative and thermal consequences of this stratospheric aerosol event. Section 2 reviews the equipment and data analysis procedures used in the study. Section 3 presents the results and compares them to other measurements. Section 4 discusses the significance of the results, especially in terms or particle transport and removal processes, and possible radiative/climatic consequences of the Fuego or similar events.

2. Instrumentation and Data Analysis

A lidar operates by firing a pulse of laser energy into the atmosphere and measuring the amount of energy scattered back by atmospheric constituents. The ground-based ruby lidar used for all observations in this study is the one used in our pre-Fuego series and was described in detail by Russell et al. (1974; 1976a,b). It produces 1- to 2-Joule pulses of wavelength 694 nm and uses a 40.6-cm (16-inch) receiving telescope. The receiver is interfaced to a computer-based digital data acquisition system that permits real-time display of signals integrated from many pulses. For each nightly observation, the lidar was operated in four or more alternating periods of low and high sensitivity, with the receiver partially obscured to produce the low-sensitivity mode. This method was used to extend the vertical range over which received signals could be accurately digitized. Both current and pulse-counting data were acquired to extend the vertical range of digitization accuracy within each sensitivity mode.

The final data analysis was performed off-line on a larger computer using the method described by Russell et al. (1974; 1976a,b). Data from all four operating modes (low-sensivity current, low-sensitivity pulse-counting, high-sensitivity current, and high-sensitivity pulse-counting) were combined to obtain a signal profile valid over an altitude range that typically extended between ~7.5 and 30 km (and above). This signal profile, together with a molecular density profile measured by

radiosonde at Oakland (32 km to the north) on the night of the lidar observation, and a stratospheric extinction profile, was used to compute a profile of scattering ratio, defined as

$$R(z) = \frac{f_p(z) + f_m(z)}{f_m(z)} = 1 + f_p(z)/f_m(z) \quad , \qquad (1)$$

where $f_p(z)$ and $f_m(z)$ are, respectively, the particulate and molecular (gaseous) backscattering coefficients at altitude z.

Because the lidar system calibration and the low-altitude atmospheric transmission are unknown, the scattering ratio profiles can initially be computed only to within an arbitrary constant. To fix this constant, each profile of R(z) is normalized to produce a statistically significant minimum value of unity. This procedure yields valid profiles, provided a level of negligibly small particulate-to-molecular backscattering ratio (f_p/f_m) exists within the altitude range of signal analysis (see Section 4 for discussion). In computing scattering ratio profiles, a particulate extinction profile must be assumed, and in this work the model of Elterman (1968) for a wavelength of 700 nm was used. This model differs from the model of negligible particulate extinction used in our 1972-74 observations, and is used to take account of the increased stratospheric particulate content observed since the eruption of Fuego (see also Section 4).

The probable error of each computed scattering ratio data point is also computed as a part of the analysis. As described in detail by Russell et al. (1974; 1976a,b) the computed error includes the probable error in lidar-measured signal, in radiosonde-measured density, and in assumed stratospheric extinction. "Error bars," equal to ± one standard error derived in this manner, are then plotted along with the measurement data, as shown below.

3. Results

The vertical profiles of scattering ratio measured in the fifteen 1975 observations are shown in Figure 1. Also shown for comparison in each frame is the average profile of scattering ratio measured between June 1973 and March 1974 in our pre-Fuego series. In each profile the excess of scattering ratio over unity may be interpreted as a type of "optical mixing ratio," as it is equal to the ratio of light backscattered by particles to that backscattered by gases [cf. Eq (1)]. Thus, for example, on 13 February at 19 km, particulate backscattering was three times as great as gaseous backscattering for the 694 nm wavelength. This very thin and intense scattering layer was evidently quite localized or short-lived, since a scattering ratio as large as four was not measured in subsequent observations either by us or by other North American observers. Nevertheless, the major increase in stratospheric particulate content caused by the Fuego eruption is obvious in all of the 1975 observations.

It is evident that the injection had its largest effect at altitudes below 20 km, thus shifting the peak altitude of scattering ratio at least several km below its immediate pre-Fuego value of 22 to 23 km. Other features of aerosol layer vertical structure revealed by the lidar measurements include a multiple-layer structure (in the early 1975 observations) that gave way to a single, broader peak; a temporary increase in particulate backscattering at the lowest stratospheric altitudes in spring; and a change in layer-top structure (near 20 km) from very abrupt

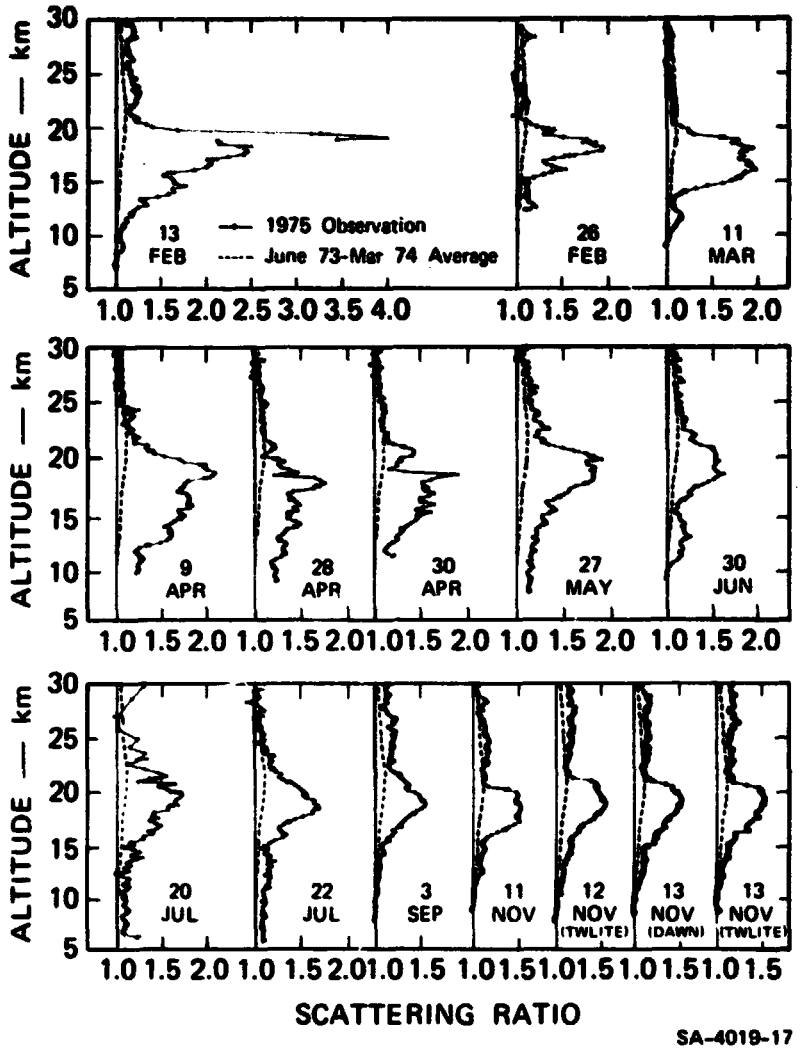

FIGURE 1 VERTICAL PROFILES OF SCATTERING RATIO MEASURED BY THE RUBY LIDAR IN 15 OBSERVATIONS, FEBRUARY-NOVEMBER 1975

The dashed profile, shown for comparison, is the average of 16 observations made in the pre-Fuego period, June 1973-March 1974.

(i.e. "flat") to more gradual, or sloping, and then back to somewhat abrupt in November 1975. All of these features are in agreement with the balloon observations made in Laramie, Wyoming, during the same period by Hofmann and Rosen (1976).

In the later 1975 profiles there is a definite increase of scattering ratio above 24 km, suggesting a gradual penetration of volcanic influence (either particles or particle-forming gases) to these altitudes. It is especially interesting to note that the November profiles, and to a certain extent the 3 September profile, have a distinct minimum in scattering ratio just above the main peak. Above this minimum a very broad secondary layer can be seen, as shown in more detail, and at higher altitudes, in Figure 2. These profile shapes, which cannot be caused by the normalization procedure, suggest a particle formation source that is above the main layer. Recently, Crutzen (1976) has described photodissociation of (possibly volcanic) carbonyl sulfide (CSO) as a possible source of sulfur above 25 km, which would lead to particle formation at those altitudes. Although the present data sample is very limited, its crude agreement with Crutzen's theory warrants further examination (see also Section 4). [Scattering ratios above 35 km are shown as dotted lines in Figure 2 because local radiosonde data on the observation dates did not extend above that altitude. At altitudes between 35 and 40 km, possible differences between actual and standard atmospheric densities are large enough

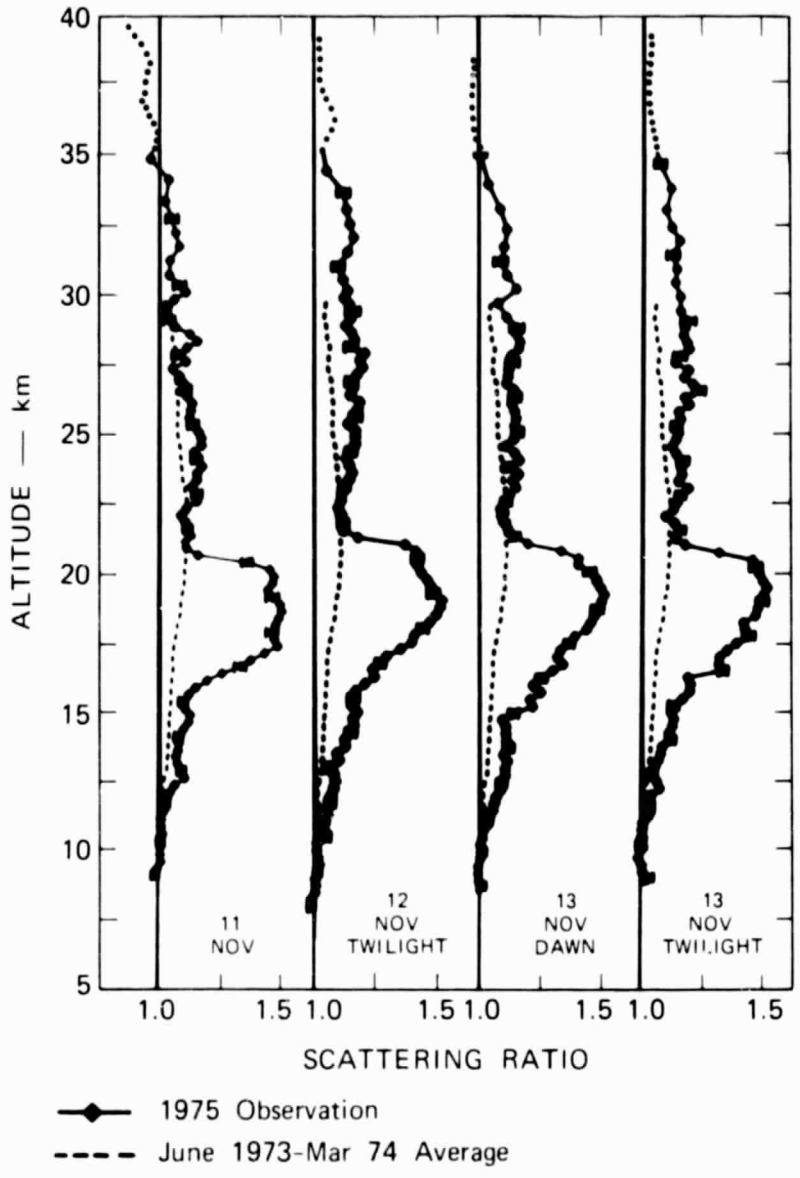

FIGURE 2 VERTICAL PROFILES OF SCATTERING RATIO MEASURED BETWEEN 11 AND 13 NOVEMBER 1975

Dotted curves, in the region above the radiosonde density measurement, were computed from the midlatitude spring-fall standard atmosphere.

(~15%) that scattering ratios computed from a standard density profile are not useful for normalization or for the purposes of Figure 2.]

One reason for making the four November observations in a period of only three days was to determine the size of day-to-day changes in layer structure. As can readily be seen from Figures 1 and 2, such changes were small, and caused primarily by vertical movements of the layer as a whole, indicating that layer structure had by November become rather stable. Within the November data set, dawn and twilight observations were made to permit a search for significant structure differences occurring between these two times of day. Again, close comparisons did not reveal any dawn-to-twilight or midnight-to-twilight differences. Finally, on an even shorter time scale, four individual portions of the 13 November dawn run, each consisting of several tens of minutes of data selected from a two-hour period, were compared in a search for systematic differences that might occur as sunlight began to impinge on the aerosol layer. This search also proved negative, as any differences that were observed did not appear to have any systematic dependence on the increasing solar illumination.

Figure 3 shows the time variation during 1975 of three different quantities that measure the predominant altitude of particulate backscattering between 10 and 30 km. These quantities are the altitude of maximum scattering ratio; the centroid of the "optical mixing ratio," R-1; and the centroid of the particulate backscattering coefficient f_p.

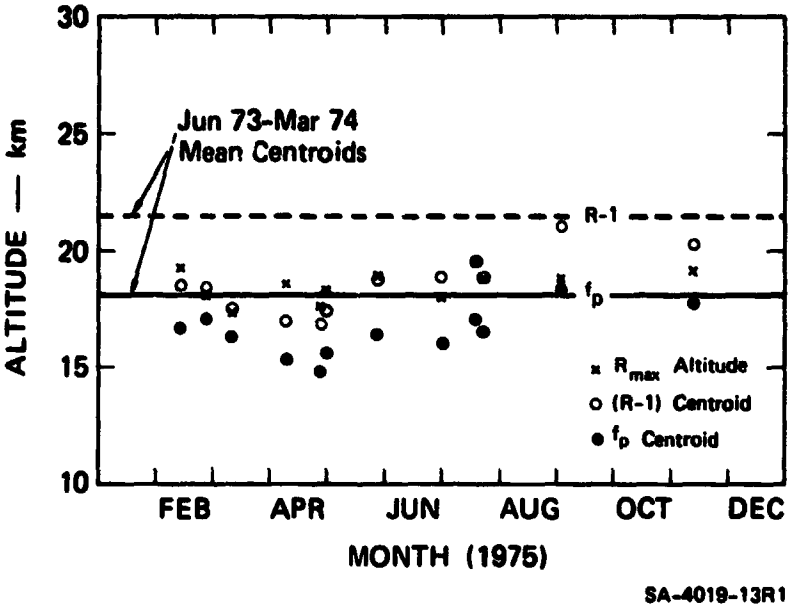

FIGURE 3 TIME VARIATION OF ALTITUDE OF MAXIMUM SCATTERING RATIO, CENTROID OF (R-1) AND CENTROID OF PARTICULATE BACKSCATTERING, FEBRUARY-NOVEMBER 1975

The centroid calculations were restricted to the altitude range 10-30 km. The altitude of R_{max} in the June 1973-March 1974 average profile is 21.9 km, or 0.5 km above the dashed line.

As expected from Figure 1, all three altitudes are consistently lower than the corresponding values observed during 1973-74. The springtime increase of scattering at the lowest stratospheric altitudes, mentioned above, is reflected by a lowering of centroids between late February and late April. After mid-April there is a gradual overall rise in centroids, as they appear to be approaching the 1973-74 values. Such a rise in centroids can be attributed to a reduction of scattering at lower altitudes

compared to higher altitudes, and is consistent with the occurrence of more efficient particle removal mechanisms at lower altitudes than at higher. As discussed by Hofmann, et al. (1975) and Hofmann and Rosen (1976), there are two possible mechanisms that tend to produce this result. One mechanism is the variations in tropopause height between late spring and early fall, which provide an effective cleansing process that is not present above 17 km. The second mechanism is particle sedimentation. This mechanism was more effective at lower altitudes than at higher, because in the post-Fuego period, as shown by Hofmann and Rosen (1976), the mean particle size between 14 and 18 km was larger than it was at higher altitudes. Faster sedimentation of larger particles therefore leads to the observed result. Again, the presence of a particle-production mechanism above the initial injection, as suggested by Crutzen (1976), could also contribute to this effect.

Figure 4 shows the behavior of maximum scattering ratio and vertically integrated particulate backscattering (10 to 30 km) over the February-November 1975 period.* An overall decline is evident in both

*The values for 26 February and 30 April have been increased somewhat (relative to the values in Figures 1 and 2) by a renormalization that forces scattering ratios above 22 km to approximate those measured in surrounding observations. This procedure is to compensate for the original normalization above 10 km, a region that the other lidar observations indicate frequently does not contain a "clean" layer suitable for normalization.

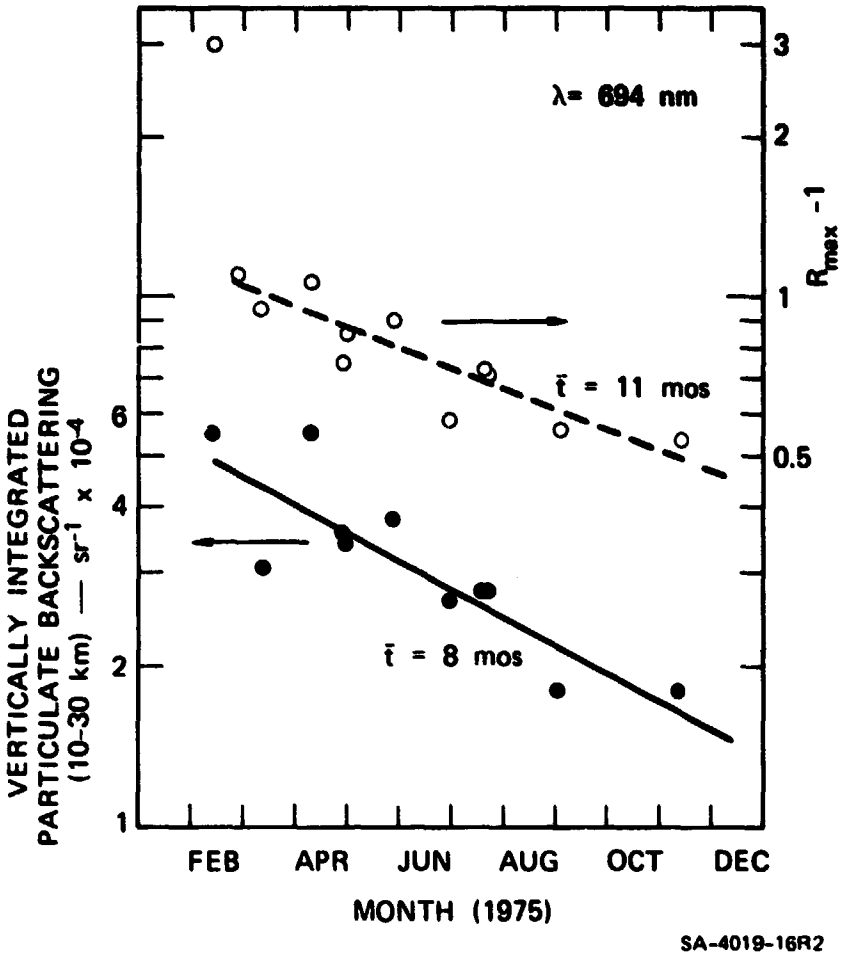

FIGURE 4 TIME VARIATION OF VERTICALLY INTEGRATED PARTICULATE BACKSCATTERING AND MAXIMUM SCATTERING RATIO, FEBRUARY-NOVEMBER 1975

The vertical integration was restricted to the altitude range 10-30 km.

quantities. After the first February observation, the maximum scattering ratio values (open circles) are fitted fairly well by an equation of the form

$$R_{max} - 1 = \left(R^{\circ}_{max} - 1 \right) e^{-t/\bar{t}} \qquad (2)$$

where the best-fit mean life, $\bar{t}$, is 11 months. This value converts to a half-life $t_{1/2}$ of 7.7 months. Prior to April, the vertically integrated particulate backscattering values (dark circles) do not decrease as regularly as do the $(R_{max} - 1)$ values (open circles). Nevertheless, the mean life of an exponential best-fit provides a useful measure of the overall rate of decline. The values thus obtained are a mean life $\bar{t}$ of 8.4 months and a half-life $t_{1/2}$ of 5.8 months. Thus vertically integrated particulate backscattering declined more rapidly than $(R_{max}-1)$. Again, this is consistent with more effective removal mechanisms below the altitude of R_{max}, because the majority of vertically integrated particulate backscattering occurred at those altitudes. (Note again the centroid altitudes in Figure 4 and the discussion thereof.)

The relation of the present postvolcanic maximum scattering ratios to those measured by a number of observers since 1964 is shown in Figure 5a. The February and 9 April 1975 values of $(R_{max} -1)$ were a factor of eight or more larger than typical values observed at SRI between June 1973 and March 1974, shortly before the Fuego volcanic eruption. Nevertheless, typical values since March 1975 have not been as large as those frequently observed by Grams and Fiocco (1967) in the years following the Agung eruption of March 1963 (see also Grams 1966). Since the 18-month observation series of Grams and Fiocco did not even begin until nine months after the Agung eruption, these data indicate that less

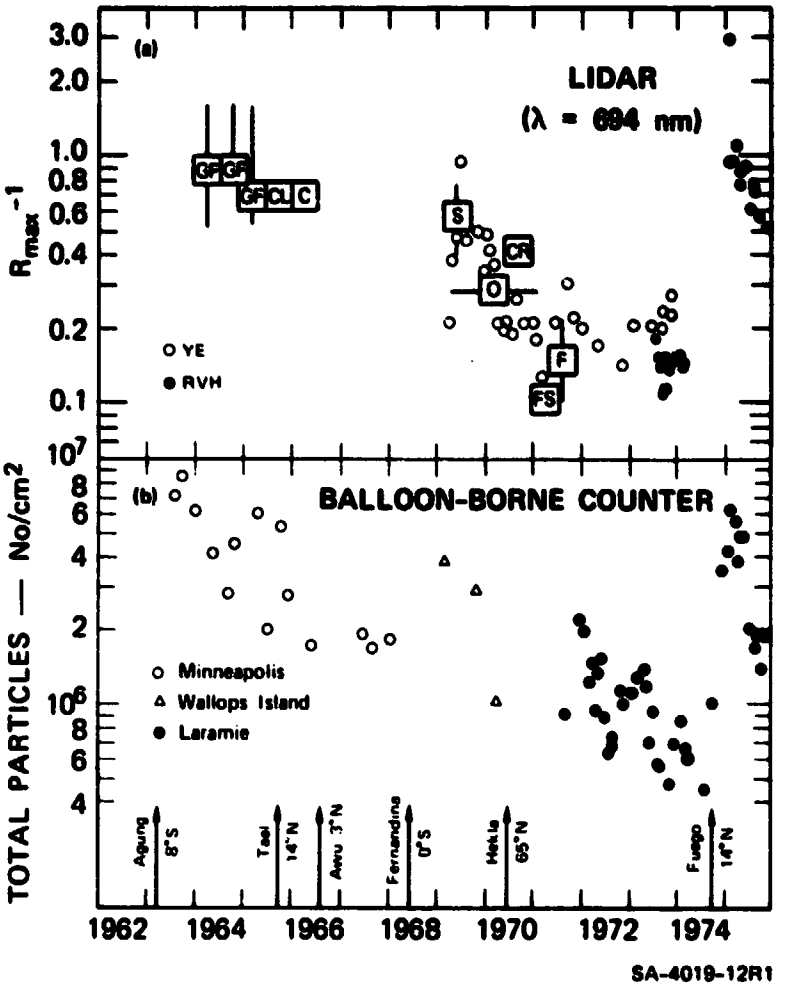

FIGURE 5 COMPARISON OF LIDAR AND BALLOON-BORNE PARTICLE COUNTER MEASUREMENTS OF THE STRATOSPHERIC AEROSOL, 1963-1975

a. Maximum ratio of particulate to gaseous backscattering measured by a number of stratospheric lidar groups. Boxes indicate mean of many observations; bars indicate range in time and magnitude. GF: Grams and Fiocco (1967), Massachusetts; CL: Collis and Ligda (1966), California; C: Clemesha et al. (1966), Jamaica; S: Schuster (1970), Colorado; CR: Clemesha and Rodrigues (1971), Brazil; O: Ottway (1972), Jamaica; FS: Frush and Schuster (unpublished), Colorado; F: Fox et al. (1973), Hawaii and Bermuda; YE: Young and Elford (1975), Australia; RVH: Present work and Russell et al. (1974, 1975b), California.
b. Number of particles (radius $\gtrsim$ 0.15 μm) above tropopause as measured by photoelectric particle counter (Hofmann et al.; 1972-74; 1973b, 1974, 1975, 1976). Arrows give times of volcanic erruptions with appreciable stratospheric penetration.

particulate and particle-forming material was introduced into the northern mid-latitude stratosphere by Fuego than by Agung.

Figure 5b shows values of the number of particles above the tropopause, as measured by balloon-borne counters flown from several Northern midlatitude sites (see references in the Figure caption). The general trend of these data parallels that of the lidar data, in showing an overall decline by an order of magnitude between 1964 and late 1974, an abrupt increase between October 1974 and early 1975, and a quite regular decline thereafter. Considering the differences between the two quantities being plotted (a point mixing ratio in Figure 5a and a vertically integrated absolute concentration in Figure 5b) and also the differences in measurement location, the overall agreement between the two data sets is very good.

It would of course be desirable to compare measured quantities that are more similar in character. However, until recently, lidar data have not been published as vertically integrated backscattering amounts, and balloon data have not been summarized as maximum mixing ratios. Fortunately, this situation is changing, and Hofmann and Rosen (1976) have recently published a time series of the maximum mixing ratio (particles per mg of air) and vertically integrated content (15 to 20 km), both as measured by balloon, in a format very similar to that of Figure 4. The agreement between the lidar and balloon data revealed in this manner is quite striking. Both the balloon-measured maximum mixing ratio and the

balloon-measured column content displayed approximately exponential declines after mid-February 1975, as did the lidar data of Figure 4. Moreover, the maximum mixing ratio had a longer mean life (12 months) than did the column content (6.6 months), again as in Figure 4. It may be significant that the balloon-measured mixing ratio lifetime was somewhat longer (by 8%) than the corresponding lidar-measured value (11 months). The difference could be caused by the stronger weighting of lidar backscattering by larger particles, which tend to fall out faster than small ones. The lidar and balloon column-content measurements cannot be compared exactly, because of their different height ranges.

Figure 6 shows the error-weighted average profile of scattering ratio for the February-November 1975 period. (The 26 February and 30 April profiles were omitted from the average because their normalization, above 10 km, makes them prone to underestimation. Moreover, only a single average profile from November was included, to avoid biasing the 1975 mean toward year-end values.) The dotted curves show the typical observational uncertainty in a single nightly observation. The dashed curves, which show the standard deviation of the profiles included in the average, indicate the large degree of variability during the nine-month period of observation, and show that most of this variability was confined to altitudes below 20 km.

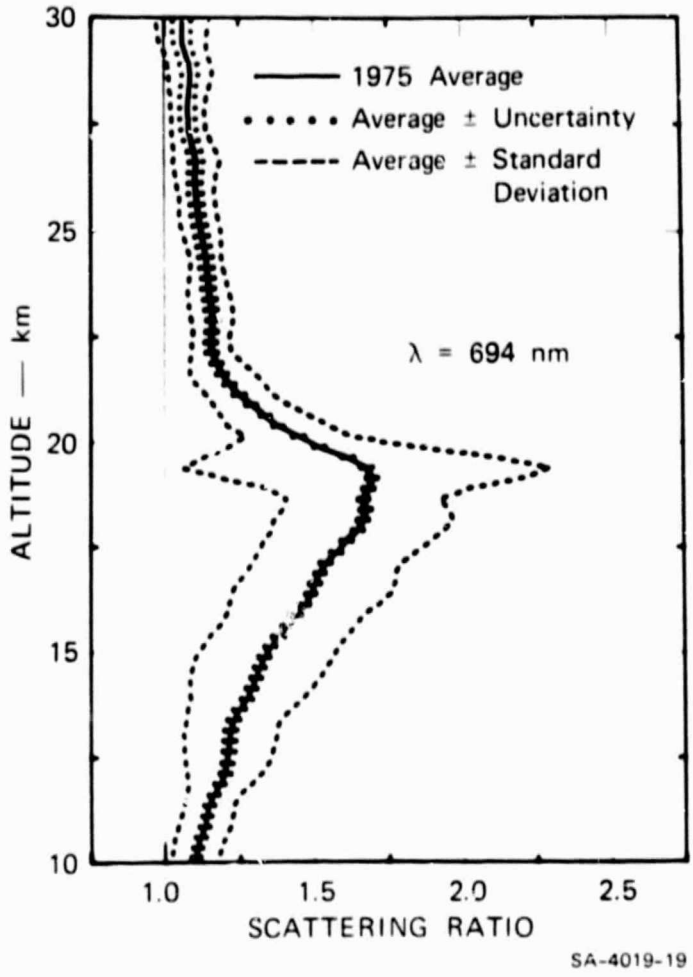

FIGURE 6 AVERAGE VERTICAL PROFILE OF SCATTERING RATIO MEASURED OVER CENTRAL CALIFORNIA COAST, FEBRUARY-NOVEMBER 1975

Solid line is error-weighed mean of 13 observations. Dotted lines indicate typical experimental uncertainty in a single profile. Dashed lines indicate standard deviation of observations included in data set.

The February-November 1975 average profile of scattering ratio is compared to our average 1973-early 1974 profile and the 1964-65 Grams and Fiocco (1967) profile in Figure 7. The large increase of particulate backscattering in the recent post-Fuego period relative to the immediate

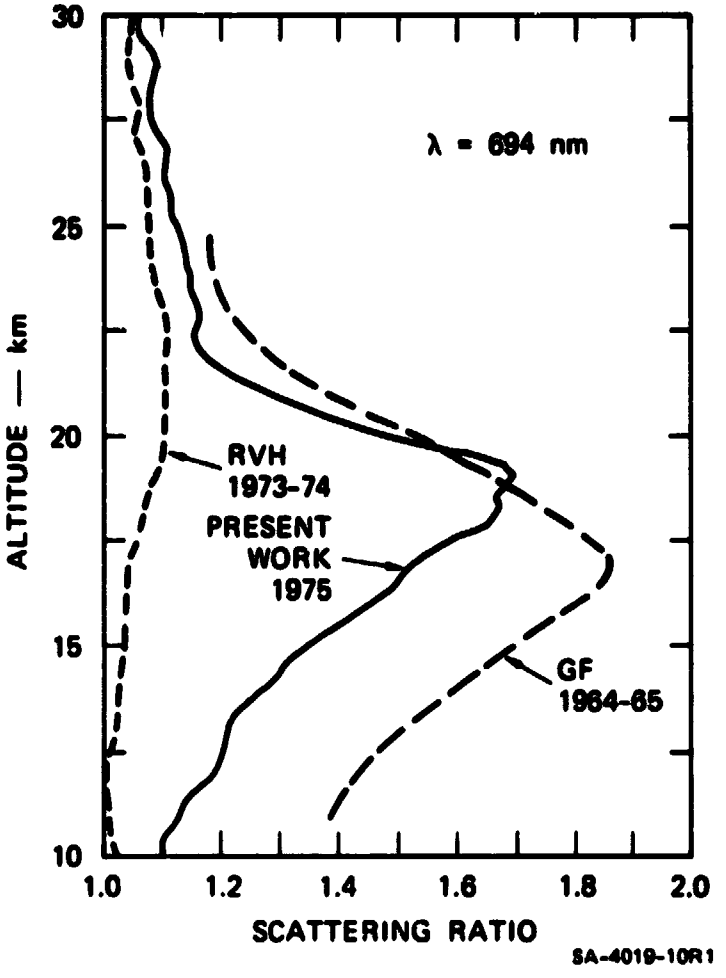

FIGURE 7 AVERAGE VERTICAL PROFILES OF SCATTERING RATIO OBSERVED IN THREE RUBY LIDAR STUDIES OF THE STRATOSPHERIC AEROSOL BETWEEN 1964 AND 1975

For references see Figure 5.

pre-Fuego period is readily evident, as is the predominantly lower altitude of the post-Fuego scattering. Nevertheless, the even larger average scattering and lower predominant altitude of the post-Agung observations are equally evident.

A characteristic of the stratospheric aerosol layer that is of primary importance to climatic studies is its optical thickness, or vertically

integrated extinction. Derivation of an optical thickness from the present lidar backscattering results requires the use of a particulate backscatter-to-extinction ratio (backscattering phase function), which has never been measured for the stratospheric aerosol. Nevertheless, useful estimates of optical thickness can be derived by using model backscattering phase functions computed for realistic optical models of the stratospheric aerosol. Recently, several such models, based on measurements, have been published (Russell et al., 1976a,b; Cadle and Grams, 1975, Pinnick et al., 1976; Toon and Pollack, 1976). Most models agree on a particle composition of concentrated sulfuric acid, except possibly just after volcanic injections. Since recent measurements indicate that the post-Fuego aerosol also was sulphuric acid (Ferry and Lem, 1975; Hofmann and Rosen, 1976), we adopt this composition in the discussion to follow.

There is less agreement on particle size distributions, probably because of different measurement methods and because of actual variability in this characteristic. (A post-Fuego increase in mean particle size has been well documented by Ferry and Lem (1976) and Hofmann and Rosen (1976). Possible size distributions include the Haze H and Haze L models of Deirmendjian (1969, 1973), a lognormal distribution derived by Pinnick et al (1976) from balloon-borne optical particle counter measurements, and a zeroth-order logarithmic distribution (Zold) derived by Toon and Pollack (1976) from a rather extensive set of measurements. Backscattering phase functions for these size distributions (for a 700-nm wavelength

and a 75% sulfuric acid refractive index of 1.42- 0i) are, respectively, 0.013, 0.018, 0.015, and 0.017 sr^{-1} (a range of ± 16% of the mean).

The range of turbidity profiles that these values yield when combined with our single 1975 average backscattering profile (Figures 6 and 7) is indicated by the shaded area in Figure 8. [Turbidity is here defined as the ratio of particulate to molecular extinction. The profiles have been converted to a wavelength λ of 550 nm assuming that particulate extinction varies as λ^{-1}, the approximate dependence displayed by the optical models of Pinnick et al. (1976).] Also shown for comparison is the turbidity profile derived by Elterman (1975) from searchlight measurements made in New Mexico in November 1974 (during the immediate post-Fuego increase) by using an assumed bistatic scattering phase function (Reeger and Seidentopf, 1946). The magnitudes of the lidar and searchlight profiles are similar, as might be expected from the time dependence shown in Figure 5. However, the altitude of the searchlight-measured turbidity maximum is about 3 km below the lidar maximum. This also is attributable to the temporal development of the Fuego injection, and is consistent with both lidar and balloon observations made in November and December 1974 (Fernald and Frush, 1975; Hofmann and Rosen, 1976).

Table 1 lists values of particulate optical thickness derived from the present and previous measurement series. As can be seen, the mean particulate optical thickness during the 1975 post-Fuego decline was about six times as large as the value in the immediate pre-Fuego years.

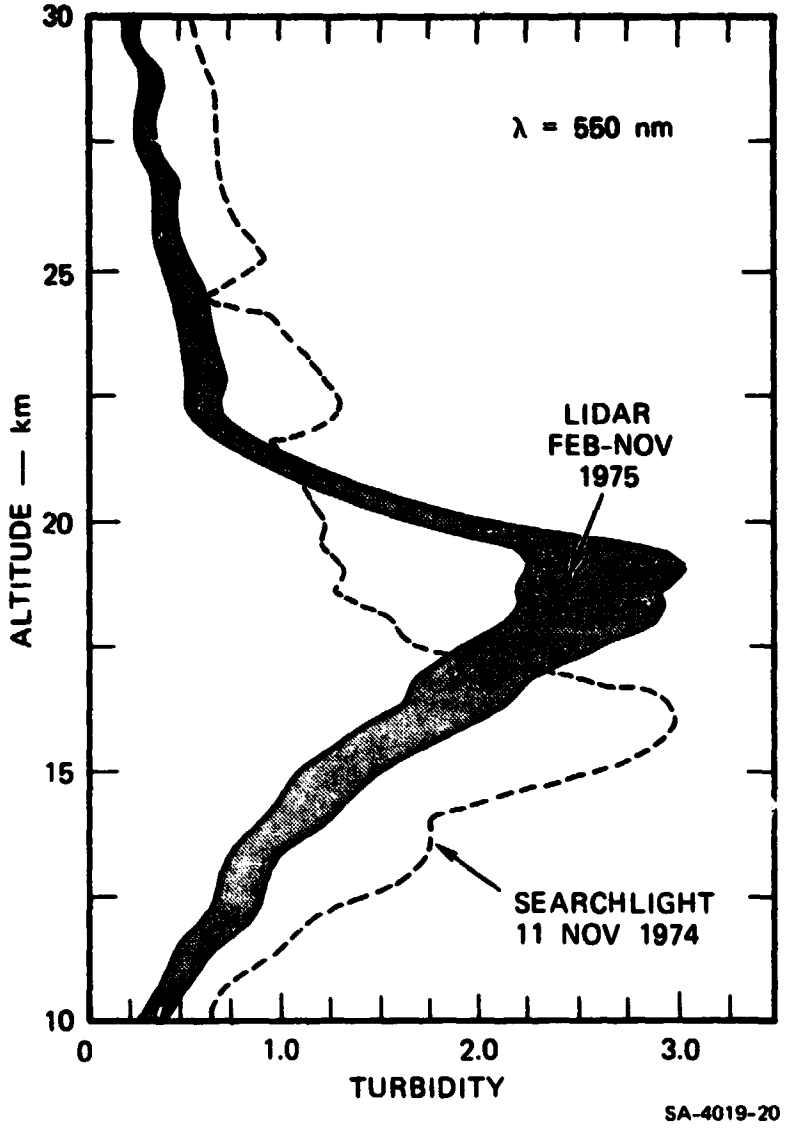

FIGURE 8 PROFILES OF STRATOSPHERIC TURBIDITY (RATIO OF PARTICULATE TO GASEOUS EXTINCTION) DERIVED FROM THE PRESENT SERIES OF LIDAR OBSERVATIONS AND FROM A SEARCHLIGHT MEASUREMENT IN LATE 1974 (ELTERMAN, 1975)

The shaded region is derived from the single average scattering ratio profile shown in Figures 6 and 7, plus a range of model backscattering phase functions.

Table 1

PARTICULATE OPTICAL THICKNESS, τ, BETWEEN 10 KM AND LISTED ALTITUDE, FOR A WAVELENGTH $\lambda \approx 550$ nm

Altitude (km)	Searchlight, April 1964-April 1965* ($\times 10^{-2}$)	Balloon, 1971-1973† ($\times 10^{-2}$)	Lidar, June 1973-Mar 1974‡ ($\times 10^{-2}$)	Compendium, "Unperturbed"§ ($\times 10^{-2}$)	Searchlight, Nov 1974** ($\times 10^{-2}$)	Lidar, Feb-Nov 1975†† ($\times 10^{-2}$)
11	0.3		0.01-0.02			0.18-0.24
12	0.6		0.04-0.05		0.6	0.37-0.50
13	0.9		0.04-0.06			0.58-0.79
14	1.2		0.07-0.10			0.80-1.1
15	1.5		0.10-0.14			1.0 -1.4
16	1.7		0.13-0.18			1.3 -1.7
17	2.0		0.16-0.22			1.6 -2.1
18	2.2		0.18-0.25			1.8 -2.5
19	2.5		0.22-0.31			2.1 -2.8
20	2.6		0.25-0.34			2.3 -3.1
21	2.8		0.27-0.38			2.4 -3.2
22	2.9		0.30-0.42			2.4 -3.2
23	2.9		0.32-0.45			2.4 -3.3
24	3.0		0.34-0.47			2.4 -3.3
25	3.0		0.35-0.48			2.5 -3.3
26	3.1		0.36-0.50		3.5	2.5 -3.3
27	3.1		0.37-0.51			2.5 -3.3
28	3.1		0.37-0.51			2.5 -3.4
29	3.1		0.38-0.52			2.5 -3.4
30	3.2	0.5-0.7	0.38-0.52	0.5	3.6	2.5 -3.4

*Elterman (1968). Based on average of bistatic searchlight measurements and model phase function.

†Pinnick et al. (1976). Based on numerous balloon-borne particle counter measurements and several realistic optical models.

‡Russell et al. (1976a,b). Based on average of 16 lidar measurements and a range of model backscattering phase functions.

§Toon and Pollack (1976). Based on lidar and sky-brightness measurements and model phase functions, plus trend of balloon, searchlight, and solar transmission measurements.

**Elterman (1975). Based on searchlight measurement and model phase function.

††Present work. Based on average of lidar measurements and range of model backscattering phase functions.

4. Discussion

a. Temporal development of aerosol structure

The temporal development of the northern midlatitude post-Fuego stratospheric aerosol observed in this study is the result of several interacting processes: transport of particles and gases from the original injection point (14.5°N, 91°W), vertical diffusion from the injection strata, gas-to-particle conversion, particle growth and sedimentation, and loss of particles below the tropopause. When this study began, in February 1975, the northern midlatitude stratospheric aerosol concentration was near its postvolcanic maximum, evidently as the combined result of northward transport of the initial injection cloud and of gas-to-particle conversion processes. A multiple-layered structure was evident in most of the February to April 1975 observations, evidently a lingering result of the original injection structure noted by many observers (e.g., Hofmann and Rosen, 1976; Hirono et al., 1975; Fernald and Frush, 1975; McCormick et al., 1975). By May the multiple layers had merged to form a single, broader layer, the centroid of which rose with time toward the altitude of the preinjection centroid. As discussed in Section 3, this upward centroid movement is consistent with the occurrence of faster particle removal at lower altitudes than at higher, as well as upward diffusion from the injection strata. The faster removal of particles at low altitudes (10-17 km) could be caused by vertical tropopause movements (Hofmann et al., 1975, Fernald and Frush, 1975b) or by

faster sedimentation of the larger particles which occurred preferentially at those altitudes (Hofmann and Rosen, 1976).

The upward centroid movement was also augmented by the formation of a broad secondary layer above the main peak, as can be seen in the September and November observations (Figures 1 and 2). The occurrence of a minimum in mixing ratio between the main and secondary layers suggests that upward diffusion is not the sole source of the secondary layer, and that a particle-formation source may be present above the main layer. As noted in Section 3, Crutzen (1976) has shown that photodissociation of volcanically injected carbonyl sulfide (CSO) could provide such a source. (See also the discussion in Section 4.c on possible normalization errors.)

Compared to some previous estimates of the residence time of stratospheric aerosols, the post-Fuego decay was rather rapid. For example, an "average residence time" or "average lifetime" of 1.5 to 2 years for stratospheric particles is frequently mentioned (e.g., Junge, 1974; Castleman, 1973), whereas the vertically integrated particulate backscattering in 1975 decayed exponentially with a mean life of only about eight months. One reason for this apparent discrepancy is the relatively low altitude at which the Fuego injection occurred. Calculations by Hunten (1975) have recently emphasized the strong dependence of particle residence times on altitude, especially between the tropopause and about 20 km. (For the case modeled by Hunten, a decrease in altitude below

(20 km by 3 km approximately halved the residence time. See also Reiter, 1975.) Further, Moore et al. (1973) concluded from measurements that stratospheric particles below 15 km have a residence time of only one to two months. Since the average 1975 centroid of particulate backscattering was near 16 km, well below preinjection values (see Figure 4), it is not surprising that the 1975 residence time was small compared to values for a nominal "20-km aerosol." The short 1975 residence time was also partially caused by the size of the 1975 particles, which was, on average, larger than preinjection values (Ferry, 1975; Hofmann and Rosen, 1976).

For these reasons the present results are not necessarily at variance with previous estimates of the residence time of typical background stratospheric particles at altitudes near 20 km. They do, however, indicate that previous estimates of the duration of influence of single volcanic injections may have been too large, at least for injections (e.g., by Agung, see Figure 7) at altitudes appreciably below the unperturbed aerosol peak. We note from Figure 5 that the decline in lidar backscattering measured in Australia after the post-Fernandina maximum had a time constant similar to that observed by both balloon and lidar after the post-Fuego maximum (also shown in Figure 5). Several other authors have already pointed out that the apparently much slower decline of the post-Agung maximum probably was the result of several subsequent smaller volcanic injections.

In the context of generalizations about the effects of volcanic injections, it should be noted that a change in dominant particle composition, from sulfate to silicate, did not occur after the Fuego eruption, although this has evidently been typical of previous eruptions (see, e.g., Cadle and Grams, 1975; Pollack et al., 1976a,b). (This fact has a bearing on our computations to follow.) Measurements made in the Fuego stratospheric plume very soon after the eruption revealed a particle composition that was predominantly sulfate, with no detectable silicate (Ferry and Lem, 1975). Four months after the eruption, a balloon measurement showed that essentially all of the stratospheric particles were volatile, again ruling out the possibility of a significant population of silicates (Hofmann and Rosen, 1976). Since the radiative properties of sulfates and silicates are significantly different, this lack of change in composition has a bearing on the radiative and climatic effects of the post-Fuego aerosol layer, as discussed below.

b. Radiative and thermal effects

The post-Fuego stratospheric aerosol layer scatters and absorbs both solar radiation and thermal infrared radiation; it therefore can modify radiation fields and temperatures in the atmosphere and at the surface. Measurements of the layer have determined particle concentration, composition, and size distribution rather well, and several radiative, or radiative/convective, models are available to use these experimental

inputs in computing the radiative and climatic effects of the layer. Although such a computation is beyond the scope of the present study, some useful estimates of the radiative and climatic effects of the post-Fuego aerosol can be derived on the basis of several modeling results already published. While the particle characteristics assumed in the published models are not exactly those of the post-Fuego layer, the model results are nevertheless useful for gauging the possible size of effects and for guiding more detailed computations.

Table 2 presents radiative and thermal properties and consequences of stratospheric aerosol layers, as computed by four recently published models. The detailed assumptions and methods used in each of the models are described in the references given in Table 2; a brief synopsis of these assumptions and methods is given in Table 3. To explain the symbols used in Table 2 we recount briefly the radiative and thermal impacts of a stratospheric aerosol layer, which is characterized in Table 2 by its mid-visible ($\lambda \approx 550$ μm) optical thickness, τ.

We first consider the effects of the layer on solar radiation. At any given time and location a fraction R of incoming solar radiation is scattered by the layer back to space. The average of this fraction over all solar zenith angles for all global locations is R_G, the global solar albedo of the stratspheric aerosol layer [row (1) of Table 2]. The particles and gases in the layer also absorb a fraction a of incoming sunlight [row (2)]. The combined effect of reflection and absorption by

Table 2

RADIATIVE AND THERMAL EFFECTS OF STRATOSPHERIC AEROSOL LAYERS, AS PREDICTED BY SEVERAL RECENT MODELS

Affected Parameter	Model			
	Cadle and Grams (1975)*	Pollack et al. (1976)†	Plumlick et al. (1976)	Harshvardhan and Cess (1975)
Solar effects				
(1) R_G	$(0.35 \pm 0.15)\tau$		0.4τ	0.37τ
(2) a (by particles)	$<0.02\tau$	0.003τ	$<0.01\tau$	≈ 0
a (by particles and gases)		0.006τ		
(3) ΔA	$(0.17 \pm 0.07)\Delta\tau$‡	$0.08\Delta\tau$	$0.2\Delta\tau$‡	$0.19\Delta\tau$‡
(4) $\Delta S/S$	$-(0.25 \pm 0.11)\Delta\tau$‡	$-0.14\Delta\tau$	$-0.28\Delta\tau$‡	$-0.26\Delta\tau$‡
Thermal infrared effects				
(5) α				0.1029τ
(6) ϵ				0.0816τ
Combined effects				
(7) ΔH_A	$(\sim 2°K\ day^{-1})\Delta\tau$ (basalt particles only)			
(8) ΔT_A			$\left\{\tau/(1 + 13.22\tau)\right\}$ 149°K§	
(9) ΔT_S	$(-6.3°K$ to $-10°K)\Delta\tau$		$-\left\{1 - \frac{[(1 - 0.37\tau)/(1 - 0.11\tau)] - 1.96 \times 10^{-11}[T_A(°K)]^{-4}\tau}{1 + 0.10\tau}\right\}$ $\times$ 162°K§	

*We have assumed an optically effective mean particle radius of 0.3 ± 0.2 μm.

†See also Toon and Pollack (1976).

‡Assumes an unperturbed system albedo A = 0.3, and no effects of increased photon path length in absorbing gases. Computed from Eqs. (3) and (4).

§Assumes an unperturbed system albedo A = 0.3, a no-particle T_A = 214°K, and R_G, α, ε as in rows (1), (5), and (6).

Table 3

PARTICLE CHARACTERISTICS AND MODELING METHODS USED IN THE MODELS CITED IN TABLE 2

Characteristic or Method	Model			
	Cadle and Grams (1975)	Pollack et al. (1976)*	Pinnick et al. (1976)	Harshvardhan and Cess (1975)
Composition	Sulfuric acid†	75% H_2SO_4, 25% H_2O		75% H_2SO_4, 25% H_2O
Refractive index (visible)	1.43-ki, $k < 0.002$‡	Palmer and Williams (1975)	1.43-ki, $k < 0.002$†	Palmer and Williams (1975)
Refractive index (infrared)		Palmer and Williams (1975)		Palmer and Williams (1975)
Size distribution	§	Zold; $r_m = 0.035$ μm, $\sigma = 2.0$	Lognormal; $r_g = 0.0725$ μm, $\sigma = 1.36$	Rosnberg (1973)
Visible radiative transfer	Single scattering, particles only	Multiple scattering (inhomogeneous doubling), particles and gases	Single scattering, particles only	Multiple scattering [Coakley and Chylek (1975)], particles only
Infrared radiative transfer	Pollack (1969), particles and gases		Newtonian cooling coefficients, particles and gases	
Surface temperature calculation	Global energy balance, plus radiative-convective equilibrium (few cases)		Global energy balance	

*See also Toon and Pollack (1976).

†Selected by us from several choices given.

‡Interpolated by us from several choices given.

§Results presented for monodisperse particles with a wide range of sizes.

the layer is, in general, to change the albedo A of the earth-atmosphere system by an amount ΔA [row (3)]. Below the stratospheric layer, the effect of this reflection and absorption is a loss of incoming solar radiation. In a sense this loss may be considered as equivalent to a reduction of the solar constant by a fraction $\Delta S/S$ [row (4)].

Since the stratospheric aerosol layer is optically thin ($\tau \ll 1$), the models yield that its albedo R_G and its fractional absorption a are directly proportional to its (mid-visible) optical thickness τ [See rows (1) and (2) of Table 2]. The system albedo change ΔA is, in the more realistic models, computed from the equation of radiative transfer by comparing the ratio of incoming and outgoing solar irradiance for perturbed and unperturbed systems. In the simplest models, which consider an isolated aerosol layer in an otherwise transparent atmosphere, this albedo change may be simply computed as (e.g., Russell and Grams, 1975):

$$\Delta A = A' - A = A\left[(1 - R_G - a)^2/(1 - AR_G)\right] + R_G - A \quad . \qquad (3)$$

In either case, the albedo change again turns out to be directly proportional to layer optical thickness τ, or to the change $\Delta\tau$ with respect to a background or unperturbed layer [See row (3) of Table 2]. Similar considerations apply to the effective reduction in solar constant $\Delta S/S$, which, for the simplest models, is given by (e.g., Cadle and Grams, 1975):

$$\Delta S/S = -R_G(1 - A) - a \quad . \qquad (4)$$

Again, for all models, the change is proportional to τ or $\Delta\tau$ [See row (4) of Table 2].

The aerosol layer also has effects in the thermal infrared, where it both absorbs and emits energy (scattering is practically negligible). Only in the model of Harshvardhan and Cess are the absorption α and emittance ϵ explicitly computed; they also are directly proportional to τ [rows (5) and (6) of Table 2]. In the model of Pollack et al. (1976a) infrared effects are determined by a solution of the radiative transfer equation (Pollack, 1969). Infrared effects of sulfuric acid particles are not considered in the models of Cadle and Grams (1975) and of Pinnick et al. (1976).

The combined effects of the stratospheric aerosol layer on solar and infrared radiation in general alter temperatures both in the vicinity of the aerosol layer itself and at the earth's surface. Changes at the aerosol layer are most pronounced in the months near the postvolcanic peak of aerosol concentration, because of the relatively short time constant (~ 100 days) of the free atmosphere for temperature changes (Pollack et al., 1976a,b). Changes at the earth's surface take longer to develop because of the long time constant (~ 4 years) of the earth-ocean system. Pollack et al. (1976a) compute both perturbed heating rates ΔH_A at the aerosol layer and surface temperature changes ΔT_S. For

optically thin layers both changes turn out to be proportional to the mid-visible optical thickness change $\Delta\tau$ [See rows (7) and (9) of Table 2]. (Unfortunately, because many past volcanic particulate injections have initially consisted predominantly of silicates, the ΔH_A computation was done for basalt particles only.) Harshvardhan and Cess (1975) provide explicit expressions for the changes ΔT_A, ΔT_S in both aerosol and surface temperatures as a function of τ [See rows (8) and (9) of Table 2]. Although formally nonlinear, these expressions also turn out to be practically linear for the optical thickness changes $\Delta\tau$ with which we will deal.

To explore the radiative and thermal consequences of the post-Fuego stratospheric aerosol layer predicted by the four models of Table 3 we adopt a mid-visible optical thickness τ of 0.030, which is the nine-month mean of our 1975 observations (Table 1). We also adopt a nonvolcanic, or unperturbed, optical thickness of 0.005, which is the unperturbed value assumed by Pollack et al. (1976a) and which falls within the range of both our pre-Fuego determinations and those of Pinnick et al. (1976) (Table 1). The results of substituting these values into the expressions of Table 2 are shown in Table 4.

The three analytical models presented in the table [Cadle and Grams (1975); Pinnick et al. (1976); Harshvardhan and Cess (1975)] agree in predicting a layer albedo R_C of about 1%; all four models show that solar absorption by the layer is negligible. The three analytical models predict an increase ΔA in system albedo that is about 1.5% of the

Table 4

RADIATIVE AND THERMAL EFFECTS OF A STRATOSPHERIC AEROSOL LAYER WITH MID-VISIBLE OPTICAL THICKNESS $\tau = 0.030$ AS PREDICTED BY THE MODELS IN TABLES 2 AND 3*

Affected Parameter	Model			
	Cadle and Grams (1975)†	Pollack et al. (1976)§	Pinnick et al. (1976)	Harshvardhan and Cess (1975)
Solar effects				
(1) R_G	0.010 ± 0.004		0.012	0.011
(2) a (by particles)	$<6 \times 10^{-4}$	9×10^{-5}	$<3 \times 10^{-4}$	≈0
a (by particles and gases)		18×10^{-5}		
(3) ΔA	0.0043 ± 0.0018‡	0.002	0.005‡	0.0048‡
(4) $\Delta S/S$	-0.0063 ± 0.0028‡	-0.0035	-0.007‡	-0.0065‡
Thermal infrared effects				
(5) a			0.0031	
(6) ε			0.0025	
Combined effects				
(7) ΔH_A	~0.05 °K day^{-1} (basalt particles only)			
(8) ΔT_A			+2.4 °K**	
(9) ΔT_S	-0.16 °K to -0.25 °K		-0.8 °K**	

*Assumes an unperturbed mid-visible stratospheric aerosol optical thickness $\tau = 0.005$; hence $\Delta\tau = 0.025$. Changes in rows (3), (4), (7), (8), (9) are with respect to the unperturbed system.

†We have assumed an optically effective mean particle radius of 0.3 ± 0.2 μm.

§See also Toon and Pollack (1967).

‡Assumes an unperturbed system albedo $A = 0.3$, and no effects of increased photon path length in absorbing gases. Computed from Eqs. (3) and (4).

**Assumes an unperturbed system albedo $A = 0.3$, a no-particle $T_A = 214$ K, and R_G, a, and ε as in rows (1), (5), and (6).

unperturbed albedo (A = 0.3). The prediction of Pollack et al. (1976a) is somewhat less than half of this value, possibly because their model accounts for increased solar absorption caused by longer photon path lengths in the absorbing gases of the aerosol layer. There is a similar difference between the numerical and analytical models in the predicted change of sublayer insolation. The analytical models predict a decrease of about 0.7%, the numerical model only about 0.35%.

Perhaps of more interest are the predicted changes of atmospheric and surface temperatures caused by the combination of solar and infrared effects. For an optical thickness increase of 0.025, the model of Pollack et al. (1976a) predicts an increased heating rate ΔH_A at the altitude of the layer, of about 0.05°K per day. Such an effect, if persistent for several months, would produce observable temperature increases. Unfortunately, the Pollack et al. (1976a) calculation was made only for basalt particles, and so does not apply specifically to the post-Fuego particles, which were sulfuric acid. On the other hand, the calculations of Harshvardhan and Cess (1975) are for sulfuric acid particles. Their model predicts an equilibrium aerosol temperature increase ΔT_A of about 2.4°K, which again might be observable by comparing average temperatures for the year before and after the Fuego eruption, or other suitable periods. The fact that the first three or four months of 1975 had optical thickness values significantly in excess of our 1975 mean of 0.03 makes such a search for a heating effect appear even more worthwhile.

(Note, however, the reservation on particle size distribution mentioned below.) Preliminary observations of such a heating effect have in fact been reported by McCormick et al. (1975) and Hirono et al. (1975). While these preliminary indications appear to be in qualitative accord with the model predictions, we do caution that stratospheric temperature changes caused by dynamic and other effects (especially breakdowns in the winter polar vortex) could overwhelm or appear to augment the purely radiative changes predicted here. See, for example, Belmont (1975).

Both the models of Pollack et al. and of Harshvardhan and Cess predict a negative change ΔT_s in equilibrium surface temperature for increased stratospheric aerosol optical thickness. (That is, the models predict that the increased solar albedo effect dominates over the increased infrared trapping or "greenhouse" effect, although the infrared effect is significant.) For a persistent layer of optical thickness 0.030 the Harshvardhan and Cess model predicts a surface temperature decrease of 0.8°K, whereas the Pollack et al. model prediction is about a factor of four less. Although a decrease of 0.8°K in surface temperature is on the threshold of detectability, it must be recalled that the long response time ($\sim$ 4 years) of the ocean-earth system will substantially diminish this decrease in the first year, and that the rapid removal rate of the post-Fuego aerosol burden ($\bar{t} \approx 8$ months) will rapidly eliminate the decrease thereafter. Feedback mechanisms (principally extension of

snow and ice cover) that are not considered in either the Harshvardhan and Cess or Pollack et al. models, are also relatively slow, so that their amplification of radiative effects, as predicted by some other models (e.g., Budyko, 1969; Sellers, 1973) would evidently not be operative in the Fuego case. Thus it seems unlikely that a demonstrable connection between any recent surface temperature changes and the post-Fuego stratospheric aerosol could plausibly be made. This result, of course, in no way rules out the general possibility of volcanic influence on surface climate; Pollack et al. (1976b) have shown that the results of larger eruptions (e.g., Krakatoa, Katmai, Agung), or of more frequent ones, could indeed be climatically significant.

While we feel that the results presented above are instructive, we also point out that the calculations can and should be improved. For example, the measured post-Fuego size distribution (Ferry, 1975; Hofmann and Rosen, 1976) should be used in place of the distributions listed in Table 3. It would also be instructive to repeat the Pollack et al. computation of ΔH_A using a sulfuric acid (rather than basalt) composition model. And, finally, since volcanic injection episodes are decidedly time-dependent, time-dependent computations for ΔT_A and ΔT_S, using the appropriate system response times, would be useful. Of course, the reasons for differing model predictions should also be explored and resolved.

c. Accuracy of the lidar results

As described in Section 3, all of our particulate backscattering values are derived by normalizing each scattering ratio profile to force its minimum value to unity. This procedure yields valid profiles provided an altitude with negligible ratio of particulate to gaseous backscattering exists within the altitude range over which signals are analyzed. If such a level does not occur, then particulate backscattering is underestimated at all altitudes (and this error is not included in the error bars of Figures 1 and 2). The magnitude of this underestimation cannot be determined from the lidar data alone, but it can be estimated by use of independent measurements of the vertical profile of particle number mixing ratio, as derived, for example, from dustsonde measurements (Hofmann et al., 1975, Hofmann and Rosen, 1976). We have previously used pre-Fuego dustsonde measurements to demonstrate that the average error introduced into our pre-Fuego backscattering values by the normalization procedure was less than 10% of the peak backscattering measured in a typical profile (Russell et al, 1976b). A similar inspection of post-Fuego dustsonde mixing ratios (Hofmann and Rosen, 1976) indicates that the average normalization error for our post-Fuego backscattering measurements was also less than 10% of profile peak backscattering values. It is true that the tropopause region in 1975 was frequently quite dirty, forcing the normalization to altitudes above the main peak, where optical mixing ratio if frequently nonnegligible; nevertheless, the very large

increase in peak backscattering during the post-Fuego period prevented the ratio of error to peak backscattering from increasing in the post-Fuego period. Thus we feel that to compensate for normalization errors any increase in the post-Fuego optical thickness values of Table 1 must be less than 10% of the listed values.

In connection with the discussion of a possible secondary layer above the main peak, it should be pointed out that the normalization procedure could also lead to an apparent, but artificial, increase of scattering above the main peak when scattering below the main peak decreases, as it did during 1975. This follows because, when scattering ratios below the main peak are larger than anywhere above the main peak--as was typical in early 1975--the normalization procedure forces the scattering ratio to unity (implying no particulate scattering) at some point above the main peak, even though actual particulate scattering may be nonzero there. Then later, as low-altitude scattering ratios decrease, the normalization altitude would move below the main peak, and scattering above the main peak could appear to increase while actually remaining at a constant, nonzero value. While we feel that this possibility is a real one and must always be kept in mind, we point out that the shapes of scattering ratio profiles are completely independent of the normalization procedure. Our statements regarding the development of a secondary layer are based primarily on the shapes of scattering ratio profiles--specifically the minimum just above the main peak and the broad, but

well-defined, hump above it, as shown in Figure 2. We therefore feel that these statements are valid regardless of any normalization ambiguities.

We have also noted in Section 2 that the Elterman (1968) extinction model was assumed in computing 1975 scattering ratio profiles. This model is in fact listed in the first column of Table 1. Comparison with the last column of Table 1 shows that, at any altitude above 10 km, the difference in two-way, 700-nm optical thickness between the model and the 1975 mean measurements was less than 0.01 (again assuming extinction $\alpha \lambda^{-1}$). This difference is the maximum relative change in scattering ratio that would result from using the last column of Table 1 in place of the first and recomputing. Even for the very last measurements made in 1975, when the difference between model and measurements was about twice this large, the change would have been less than the error bars shown in Figures 1 and 2, which are about ± 3%. The resulting change in vertically integrated backscattering (hence turbidity and optical thickness) would have been negligible.

5. Summary

Our 1975 stratospheric lidar observations began at about the peak of northern midlatitude influence of the Fuego volcanic injection. Multiple-layered structure, observed by others since the time of the eruption, was still present in early 1975, but by May the individual layers had merged to form a single, broader layer. The increase in particulate backscattering resulting from the volcanic injection was confined almost entirely to altitudes below 20 km. As a result, layer centroids in 1975 were typically several km below their altitudes prior to the eruption. After April 1975 the centroids gradually rose toward their preinjection value, as particles at the lowest stratospheric altitudes were removed faster than those at higher altitudes. Toward the end of our 1975 observations, profile shapes suggest the formation of a secondary, broad layer above the main peak. A search for dawn-to-twilight differences in layer structure, and for differences caused by the rising sun, revealed no changes that were systematically different from those commonly observed during other time periods of similar length.

From late February on, both vertically integrated particulate backscattering and the peak ratio of particulate to gaseous backscattering displayed approximately exponential declines, with mean lifetimes of 8 and 11 months, respectively. Very similar behavior was observed by balloon-borne particle counters in Wyoming during the same period

(Hofmann and Rosen, 1976). The relatively short residence times are a combined result of the low altitude of the volcanic injection and of the larger mean particle size of the postvolcanic aerosol with respect to the prevolcanic or "background" aerosol.

The 1975 mean profile of scattering ratio had a maximum value of 1.7, and vertically integrated particulate backscattering (10-30 km) of 3.6×10^{-4} sr^{-1} (both for $\lambda = 694$ nm). When combined with several realistic optical models of the sulphuric acid particles, this backscattering yields a mean mid-visible ($\lambda \approx 550$ nm) optical thickness of 0.03 ± 0.005. This value is about a factor of six larger than the preinjection optical thickness, but smaller than values observed in northern midlatitudes for several years following the Agung eruption of 1963.

Radiative and thermal consequences of the measured post-Fuego layer were computed using several recently published models. The models yield a global albedo for the 1975 mean layer of about 1%, or possibly smaller because of gaseous absorption of photons scattered in the layer. The derived increase in earth-atmosphere system albedo was between 0.002 and 0.005. The models predict that infrared absorption by the sulfuric acid particles could increase temperatures at the aerosol layer altitudes by several degrees K. They predict a decrease in surface temperature (that is, increased solar albedo dominates over increased infrared trapping), but the decrease is considerably smaller than $1^{\circ}K$, both because of the small optical thickness of the volcanic layer and because of its short residence time relative to the earth-ocean thermal response time.

ACKNOWLEDGMENTS

We are grateful to D. J. Hofmann for releasing his balloon data prior to publication, to G. V. Ferry for particle size distribution data, to D. Colburn for particle phase function values, and to J. B. Pollack and F. E. Volz for useful discussions and prepublication results. At SRI, J. Knotts, J. van der Laan, and P. Rozario played major roles in lidar operation and data reduction.

This research was supported by the U.S. Department of Transportation through a contract administered by the Ames Research Center of the National Aeronautics and Space Administration.

REFERENCES

Belmont, A. D., 1975: Variability of stratospheric winds and temperature. Section 2.3 of The Natural Stratosphere of 1974, A. J. Grobecker, ed., Report DOT-TST-75-51. Available from NTIS, Springfield. Virginia.

Budyko, M. I., 1969: Climatic change. Sov. Geog., 10, 429-457.

Cadle, R. D., and G. W. Grams; 1975: Stratospheric aerosol particles and their optical properties. Rev. Geophys. Space Phys. 13, 475-501.

Castleman, A. W., Jr., H. R. Munkelwitz, and B. Manowitz, 1973: Contribution of volcanic sulfur compounds to the stratospheric aerosol layer. Nature, 244, 345-346.

Clemesha, B. R., G. S. Kent, and R.W.H. Wright, 1966: Laser probing of the lower atmosphere. Nature, 237, 328-329.

Clemesha, B. R., and S. N. Rodrigues, 1971: The stratospheric scattering profile at 23° south. J. Atmos. Terr. Phys., 33, 1119-1124.

Coakley, J. A., Jr., and P. Chýlek, 1975: The two-stream approximation in radiative transfer: including the angle of the incident radiation. J. Atmos. Sci., 32, 409-418.

Collis, R.T.H., and M.G.H. Ligda, 1966: Note on lidar observations of particulate matter in the stratosphere. J. Atmos. Sci., 23, 255-257.

Crutzen, P. J., 1976: The possible importance of CSO for the sulfate layer of the stratosphere. Geophys. Res. Lett. 3, 73-76.

Deirmendjian, D., 1969: Electromagnetic scattering on spherical polydispersions. American Elsevier.

Deirmendjian, D., 1973: On volcanic and other particulate turbidity anomalies. Adv. in Geophys., 16, 267.

Elterman, L., 1968: UV, Visible and IR attenuation for altitudes to 50 km, 1968. AFCRL-68-0153, Env. Res. Paper No. 285. Air Force Cambridge Research Laboratory, Bedford, Massachusetts.

_____, 1975: Stratospheric aerosol parameters for the Fuego volcanic incursion. Appl. Opt., 14, 1262-1263.

Fegley, R. W., and H. T. Ellis, 1975: Lidar observations of a stratospheric dust cloud layer in the tropics, Geophys. Res. Lett., 2, 139.

Fernald, F. G., and C. L. Frush, 1975a: Lidar observations of the enhanced stratospheric dust layer associated with the eruption of volcano de Fuego, EOS Trans., Amer. Geophys. Union, 56, 366.

_____, 1975b: Observations of Fuego dust over Boulder, Colorado. Conf. Abstracts, Seventh Int. Laser Radar Conf., Menlo Park, California, 4-7 November. Available from Stanford Research Institute.

Ferry, G. V., 1975: Personal communication.

Ferry, G. V., and H. Y. Lem, 1975: Changes in stratospheric aerosols collected after the eruption of volcano de Fuego. EOS Trans. Amer. Geophys. Union, 56, 366.

Fox, R. J., G. W. Grams, B. G. Schuster, and J. A. Weinman, 1973: Measurements of stratospheric aerosols by airborne laser radar. J. Geophys. Res., 78, 7789-7801.

Grams, G. W., 1966: Optical radar studies of stratospheric aerosols. Thesis, Dept. of Meteorol., Mass. Inst. of Tech.

Grams, G. W., and G. Fiocco, 1967: Stratospheric aerosol layer during 1964 and 1965. J. Geophys. Res., 72, 3523-3542.

Harshvardhan and R. D. Cess, 1975: Stratospheric aerosols: effect on atmospheric temperature and global climate. Collection of Abstracts, Second Conf. Atmos. Radiation, Arlington, Virginia, 29-31 October 1975. Amer. Meteor. Soc.

Hirono, M., M. Fujiwara, and T. Itabe, 1975: Lidar observations of stratospheric aerosol content after the eruption of the Fuego volcano. Conf. Abstracts. Seventh Int. Laser Radar Conf., 4-7 November 1975, Menlo Park, California. Available from Stanford Research Institute.

Hofmann, D. J., J. M. Rosen, T. J. Pepin, and R. G. Pinnick, 1975: Stratospheric aerosol measurements I: time variations at northern midlatitudes. J. Atmos. Sci., 32, 1446-1456.

Hofmann, D. J., and J. M. Rosen, 1976: Balloon observations of the time development of the stratospheric aerosol event of 1974-75. Dept. of Physics and Astronomy, Univ. of Wyoming. See also EOS Trans. Amer. Geophys. Union (1975).

Hofmann, D. J., J. M. Rosen, T. J. Pepin, and J. L. Kroening, 1972: Global monitoring of stratospheric aerosol, ozone, and water vapor. Progress Report, June 1972, Dept. of Physics and Astron., Univ. of Wyoming.

_____, 1973: Global monitoring of stratospheric aerosol, ozone, and water vapor. Progress Reports, April and June 1973. Dept. of Physics and Astron., Univ. of Wyoming.

_____, 1974a: Global monitoring of stratospheric aerosol, ozone, and water vapor. Progress Report, February 1974. Dept. of Physics and Astron., Univ. of Wyoming.

Hunten, D. M., 1975: Residence times of aerosols and gases in the stratosphere. Geophys. Res. Lett., 2, 26-28.

Junge, C. E., 1974: Important problems of global pollution. Proc. Int. Conf. on Structure, Composition and General Circulation of the Upper and Lower Atmospheres and Possible Anthropogenic Perturbations, Melbourne, Astralia, 14-25 January 1974. N. J. Derco and E. J. Truhaler, eds., IAMAP.

Lazrus, A. L., B. W. Gandrud, R. N. Woodard, and W. A. Sedlacek, 1975: Stratospheric sulfate and other constituents by volcan de Fuego. EOS Trans., Amer. Geophys. Union, 56, 366.

McCormick, M. P., and W. H. Fuller, Jr., 1975: Lidar measurements of two intense stratospheric dust layers, Appl. Opt., 14, 4.

McCormick, M. P., W. H. Fuller, Jr., W. P. Chu, and T. J. Swissler, 1975: Stratospheric lidar measurements of the Fuego volcanic event. Seventh Int. Laser Radar Conf., Menlo Park, California, 4-7 November.

Meinel, A. B., and M. P. Meinel, 1974: A stratospheric dust/aerosol event of November 1974. Science, 188, 477.

Moore, H. E., S. E. Poet, and E. A. Martell, 1973: ^{222}Rn, ^{210}Pb, ^{210}Bi, and ^{210}Po profiles and aerosol residence time versus altitude. J. Geophys. Res., 78, 7065-7075.

Ottway, N. T., 1972: Laser radar observations of the 20-km aerosol layer. Fourth Conf. on Laser Atmos. Stud., Tucson, Arizona, 1972.

Palmer, K. F., and D. Williams, 1975: Optical constants of sulfuric acid; application to the clouds of Venus? Appl. Opt., 14, 208-219.

Pepin, T. J., 1975: Solar extinction measurements of stratospheric aerosols in 1975. EOS Trans., Amer. Geophys. Union, 56, 366.

Pinnick, R. G., J. M. Rosen, and D. J. Hofmann, 1976: Stratospheric aerosol measurements III: optical model calculations. J. Atmos. Sci., 33, 304-314.

Pollack, J. B., 1969: Temperature structure of nongrey planetary atmospheres. Icarus, 10, 301-313.

Pollack, J. B., O. B. Toon, C. Sagan, A. Summers, W. Van Camp, and B. Baldwin, 1975: Stratospheric aerosols and climatic change. Submitted to Science.

Pollack, J. B., O. B. Toon, A. Summers, W. Van Camp, and B. Baldwin, 1976a: Estimates of the climatic impact of aerosols produced by space shuttles, SSTs, and other high flying aircraft. J. Appl. Meteor., 15, 247-258.

Pollack, J. B., O. B. Toon, C. Sagan, A. Summers, B. Baldwin, and W. Van Camp, 1976b: Volcanic explosions and climatic change: a theoretical assessment. J. Geophys. Res., 81, 1071-1083.

Reeger, E., and F. Seidentopf, 1946: Die Streufunktion des atmosphärichen dustes nach Scheinwerfermessungen, Optik, 1, 18.

Reiter, E. R., 1975: Mean structure of the stratosphere. Section 2.2 of The Natural Stratosphere of 1974, A. J. Grobecker, ed., Report DOT-TST-75-51. Available from NTIS, Springfield, Virginia.

Remsberg, E. E., 1973: Stratospheric aerosol properties and their effects on infrared radiation. J. Geophys. Res., 78, 1401-1408.

Remsberg, E. E., and G. B. Northam, 1975: Measurements of stratospheric dust over Virginia by laser radar. EOS Trans., Amer. Geophys. Union, 56, 365.

Rosen, J. M., D. J. Hofmann, and J. Laby, 1975: In-situ measurements of the recent increase in stratospheric aerosol. EOS Trans., Amer. Geophys. Union, 56, 365.

Russell, P. B., and G. W. Grams, 1975: Application of soil dust optical properties in analytical models of climate change. J. Appl. Meteorol., 15, 1037-1043.

Russell, P. B., W. Viezee, and R. D. Hake, Jr., 1974: Lidar measurements of the stratospheric aerosol over Menlo Park, California; October 1972-March 1974. Final Report 2217, Stanford Research Institute.

_____, 1976a: Lidar observations of the stratospheric aerosol: California, October 1972-March 1974. Quart. J. Royal Meteor. Soc., in press.

_____, 1976b: Lidar observations of the stratospheric aerosol: summary of results and a calibration error assessment. Proceedings, Fourth Conf. Climatic Impact Assessment Prog., Cambridge, Massachusetts, 4-7 February 1975. U.S. Dept. of Transportation, in press.

Sellers, W. D., 1973: A new global climatic model. J. Appl. Meteor., 12, 241-254.

Schuster, B. G., 1970: Detection of tropospheric and stratospheric aerosol layers by optical radar (lidar). J. Geophys. Res., 75, 3123-3132.

Smithsonian Institute, 1974: Center for Short-Lived Phenomena, Event Card #139-74.

Toon, O. B., and J. B. Pollack, 1976: A global average model of atmospheric aerosols for radiative transfer calculations. J. Appl. Meteor., 15, 225-246.

Volz, F. E., 1975: Volcanic twilights from the Fuego eruption. Science, 189, 48-50.

Young, S. A., and W. G. Elford, 1975: Laser observations of stratospheric aerosols at Adelaide (35°S), 1969-73. Internal Report ADP 119, Dept. of Physics, University of Adelaide, Adelaide, Australia.